

Quantum Plasmonics: Nonlocal effects in coupled nanowire dimer.

T.V. Teperik¹, P. Nordlander², J. Aizpurua³ and A. G. Borisov^{4*}

¹ *Institut d'Electronique Fondamentale, UMR 8622 CNRS-Université Paris-Sud,
Bâtiment 220, 91405 Orsay Cedex, France.*

² *Department of Physics and Astronomy,
M.S. 61 Laboratory for Nanophotonics, Rice University,
Houston, Texas 77251-1892, USA.*

³ *Material Physics Center CSIC-UPV/EHU and
Donostia International Physics Center DIPC,
Paseo Manuel de Lardizabal 5 20018, Donostia-San Sebastián, Spain*

⁴ *Institut des Sciences Moléculaires d'Orsay, UMR 8214 CNRS-Université Paris-Sud,
Bâtiment 351, 91405 Orsay Cedex, France.*

E-mail: andrei.borisov@u-psud.fr

Abstract

The optical response of a coupled nanowire dimer is studied using a fully quantum mechanical approach. The translational invariance of the system allows to apply the time-dependent density functional theory for the plasmonic dimer with the largest size considered so far in quantum calculations. Detailed comparisons with results from classical electromagnetic calculations based on local and non local hydrodynamic response, as well as with results of the recently developed quantum corrected model is performed. We show that electron tunneling

*To whom correspondence should be addressed

and dynamical screening are the major nonlocal quantum effects determining the plasmonic modes and field enhancement in the system. Account for the electron tunneling at small junction sizes allows semi-quantitative description of quantum results within classical framework. We also discuss the shortcomings of classical treatments using non-local dielectric permittivities based on hydrodynamic models. Finally, the implications of the actual position of the screening charge density for the plasmon ruler applications are demonstrated.

KEYWORDS Nanoparticle dimer, quantum plasmonics, field enhancement, plasmon ruler

In metal nanoparticles, collective excitation of the valence electrons induced by an incident electromagnetic field, the localized plasmon, leads to plethora of optical phenomena of significant current interest. For instance, strong plasmonic enhancement of the local fields¹⁻⁵ opens a route to numerous practical applications, such as surface enhanced Raman scattering (SERS),⁶⁻⁹ optical nano-antennas^{10,11} allowing, for example, the control of radiation from single quantum emitters,¹² or generation of extreme ultraviolet pulses by non-linear high harmonic generation.¹³ In nanoparticle assemblies, the hybridization of plasmonic modes can serve for guiding of the propagating fields,^{14,15} as well as it offers a way for rational engineering of desired optical response and local field profile.⁴ Not only light harvesting and sensing properties can be thus greatly improved, but also the specific geometry dependence of the optical response can be used as plasmon ruler to determine the arrangement and nanoscale distances within chemical or biological species.^{4,16-21}

Significant advances in fabrication and manipulation techniques allow nowadays for precise control of the geometry of the structure.²¹⁻²⁹ In particular, for nanoparticle assemblies the size of the gap between the adjacent nanoparticles can be brought below one nanometer so that the electron tunneling across the junction becomes possible. Thus, the plasmonic devices enter the quantum regime which represents a significant challenge for available theoretical approaches. Indeed, most of the descriptions of the optical response are based on the solution of the classical Maxwell equations where the nanoparticles are modeled with sharp surfaces and the quantum nature of electrons forming the screening charge is neglected. Such effects as experimentally observed appearance

of the charge transfer plasmon for conductively coupled particles prior to direct contact,^{28,29} or optical rectification^{23,30} can not be addressed within a classical framework. As shown with recent quantum calculations^{28,31–34} the main ingredients missing in the classical model are the spill out of conduction electrons outside the nanoparticle surfaces, and the finite spatial profile of the plasmon-induced screening charge. The use of a nonlocal dielectric functions^{2,35–43} can account for the latter effect, where the variation of electron density is smooth rather than infinitely sharp, as assumed in the classical local approach. However, the spill out of electrons outside the nanoparticle surfaces and associated tunneling across the narrow interparticle junctions requires special treatment.

In this respect, the data available on the coupled nanoparticle dimer is quite revealing. This is a prototypical system for plasmonic nanoparticle coupling, which has been extensively studied.^{2–4} Theoretical studies based on the solution of the classical Maxwell equations predict a discontinuous transition from the capacitively to conductively coupled particles. For vanishing junction size, the fields in the junction diverge and the plasmon modes experience diverging red shift as a result of the interaction between high charge densities induced at the opposite sides of the junction.^{3–8,44–46} The charge transfer plasmon appears abruptly after the conductive contact.^{45,47} The nonlocal calculations based on the hydrodynamic model^{2,35,36,40–42} have shown that because of the finite spatial profile of the plasmon-induced screening charge, the fields in the junction stay finite albeit large. The number of plasmon resonances and their frequency shift is much reduced compared to classical predictions. On the other hand, it follows from the quantum treatments^{28,31–33} that for narrow junctions, electron tunneling can short circuit the junction and quench the plasmon-induced field enhancement. The nanoparticles appear conductively connected prior to direct contact, and the transition between the non-touching and conductive contact regimes is continuous. In particular, the charge transfer plasmon associated with interparticle charge transfer^{48–52} progressively emerges in the optical response of the system, as has been fully confirmed in recent experiments.^{28,29} These quantum effects could be reproduced with Quantum Corrected Model (QCM)³³ that treats the junction between the nanoparticles as an effective medium allowing to account for

the quantum effects within the classical local Maxwell theory.^{28,29}

Present situation is thus characterised by the experimental ability to create the structures with sub-nanometer characteristic scales and several sometimes controversial theoretical approaches to address the optical properties of such a nanostructures. While quantum calculations provide an *a priori* exact answer to the problem, to date the application of rigorous quantum mechanical approaches to coupled plasmonic systems have been limited to rather small systems and are extremely heavy numerically. It is thus of considerable interest to have a bench mark quantum results on possibly large realistic system of coupled plasmonic particles allowing detailed comparison between full quantum and macroscopic Maxwell theories. This would allow to assess of the role of quantum mechanical effects and of the possibility to account for these effects in classical theory. In this article which concerns a strongly coupled nanowire dimer, we offer such a comparison. We show that the quantum mechanical results for the optical response of the system can be quantitatively reproduced with simple models. *Local classical* description of the system allows to account for the interparticle tunneling through the narrow junction and for the actual location of the dynamically induced screening charges.

Model and computational aspects

The system considered in this work consists of two identical nanowires in vacuum. The nanowires are infinitely extended along z -axis as sketched in Fig. 1. Each nanowire has a circular cross-section of diameter D . The nanowires are separated by a variable distance S and the incident light is polarized along the inter-particle axis x . Coupled nanowires and nanorods are often used in SERS, nanoantenna, and plasmon guiding applications.^{3,4,10,11,20,24,53–57} Thus, this system is well characterized both from experimental and theoretical point of view. Full numerical studies based on the solution of the classical Maxwell equation have been performed,^{24,47,58–62} as well as semi-analytical studies based on transformation optics.^{40,41,63} The system has also been investigated using non-local hydrodynamic description.^{40–43} The high symmetry of the system with its

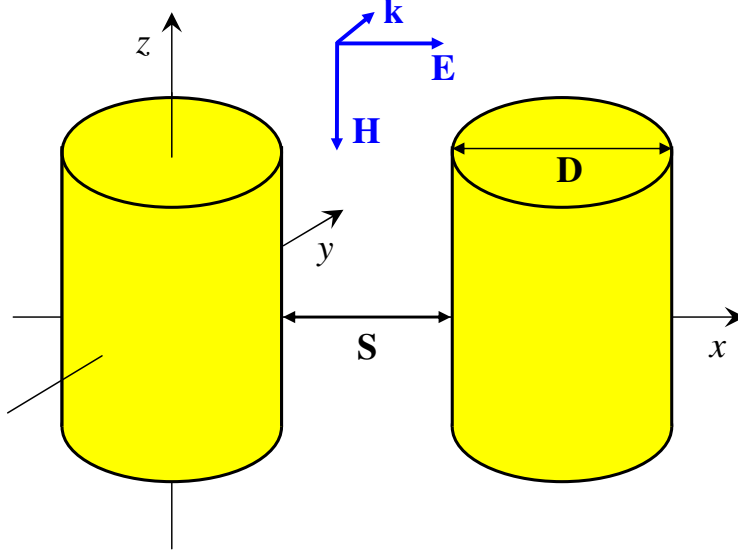


Figure 1: Sketch of geometry of the nanowire dimer. Two identical cylindrical nanowires are infinite along z -axis and have diameter D of the circular cross-section in the (x, y) - plane. The nanowires are separated by the junction of width S . The incident radiation is linearly polarised with electric field along x -axis.

translational invariance along the z -axis allows us to address on the full quantum level the case of the cylinders with $D = 9.8$ nm. To our knowledge this is the largest size of the plasmonic dimer described so far within the time dependent density functional theory (TDDFT) framework.

For the nanowires we adopt the cylindrical jellium model (JM). Despite its simplicity, this model captures the collective plasmonic modes of the conduction electrons and has demonstrated its predictive power for quantum effects in nanoparticle dimers.^{28,29} While obviously not providing chemical accuracy, the JM is well suited for the description of the nonlocal effects due to conduction electrons such as dynamical screening of external field and tunneling as we discuss below. Along with the possibility to treat relatively large system on a full quantum level, the JM model allows for direct comparison between quantum and classical electromagnetic theory results. Indeed, the physics underlying the Drude model for the metal response as well as the refinement of the Drude model introduced by the nonlocal hydrodynamic model corresponds best to free electron metals. For noble metals, such as silver and gold, the contribution of the localised d -electrons to the screening would obscure the comparison.

Within the JM, the ionic cores of the nanowire atoms are represented with uniform back-

ground charge density $n_0 = \left(\frac{4\pi}{3} r_s^3\right)^{-1}$. The screening radius r_s is set equal to $4 a_0$ (Bohr radius $a_0=0.053$ nm) corresponding to Na metal. Sodium is a prototype system for which the JM performs particularly well in description of the finite size non-local effects on optical properties.⁶⁴ It should be emphasized that the qualitative conclusions drawn in this work are robust and independent of the particular choice of density parameter. Each of nanowires is characterised by the number of electrons N_e per unit length so that from the charge neutrality the nanowire diameter is $D = 2\sqrt{4N_e r_s^3/3}$. The circle of diameter D provides the position of the jellium edge separating uniform positive background from the vacuum. The jellium edge is located at half a lattice constant a ($a = 4.23$ Å for Na) in front of the last atomic plane at the surface. We have performed calculations for $N_e = 40$ and $N_e = 100$ with $D_{40} = 6.2$ nm and $D_{100} = 9.8$ nm respectively. The Fermi energy in both cases is at 2.9 eV below the vacuum level.

The quantum calculations of the absorption cross-section are based on the Kohn-Sham (KS) scheme of the time-dependent density functional theory (TDDFT).⁶⁵ We use the adiabatic local density approximation (ALDA) with the exchange-correlation functional of Gunnarson and Lundqvist.⁶⁶ Retardation effects can be neglected due to the small size of the system. Extended description of present numerical implementation can be found in Ref.³² Therefore we only discuss here specific aspects linked with present work on interacting nanowires. In brief, the Kohn-Sham orbitals of the ground state of interacting dimer $\psi_j(x, y)$ are obtained from these of non-interacting distant cylinders by adiabatically reducing the separation. The $\psi_j(x, y)$ are discretized on the equidistant mesh in cartesian coordinates, and the time dependent Kohn-Sham equations

$$i \frac{\partial \Psi_j(x, y, t)}{\partial t} = \left(-\frac{\Delta}{2m} + V_{\text{eff}}(x, y, t; [n]) \right) \Psi_j(x, y, t) \quad (1)$$

are then solved with initial conditions $\Psi_j(x, y, t = 0) = \psi_j(x, y)$. In Eq. (1) m is the free electron mass, and $\Delta = \partial^2/\partial x^2 + \partial^2/\partial y^2$. The effective potential of the system V_{eff} depends on the electron

density $n(x, y, t)$ given by:

$$n(x, y, t) = 2 \sum_{j \in occ.} \chi_j |\Psi_j(x, y, t)|^2. \quad (2)$$

The sum runs over occupied states, the factor 2 results from the spin degeneracy, and χ_j is the number of electronic states associated with z -motion along the nanowire.

$$\chi_j = \frac{1}{\pi} \sqrt{2(E_F - E_j)}, \quad (3)$$

where E_F is the Fermi energy, and E_j is the energy of the $\psi_j(x, y)$ orbital.

The dipole absorption cross-section per unit length is calculated from the density dynamics induced by impulsive perturbation as: $\sigma_{abs}(\omega) = \frac{4\pi\omega}{c} \text{Im} \{ \alpha(\omega) \}$, with $\alpha(\omega)$ being the dipolar polarizability (per unit length) of the system, and c - speed of light in vacuum. In order to analyse the temporal evolution of the system corresponding to the excitation of the given plasmonic resonance we perform the TDDFT calculations for the nanowire dimer subjected to an incident x -polarized laser pulse. Electric field of the pulse is given by $E_L(t) = E_0 \exp \left[- \left(\frac{t-T}{0.2T} \right)^2 \right] \cos \Omega t$. The frequency of the pulse Ω is set resonant with studied plasmonic mode. The duration of the pulse T (typically 50 fs) is large enough for the narrow spectral width. The amplitude E_0 is any small number to guarantee the linear response regime.³² The snapshots of the induced densities, currents and fields presented lower in this paper are extracted at $t \sim T/2$.

The classical electromagnetic calculations of the absorption cross-section have been performed with Comsol Multiphysics package, (version 4.2a, www.comsol.com). Local, nonlocal, and quantum corrected model description of the dielectric properties of the system were used. It is noteworthy that because of the small size of the plasmonic dimer the absorption cross-section closely correspond to extinction cross-section in this case.

Within the local classical approach the dielectric constant of the nanowires is described with Drude model, which is a good approximation for the free electron metal as sodium considered in

this work.

$$\varepsilon(\omega) = 1 - \frac{\omega_p^2}{\omega(\omega + i\gamma)}, \quad (4)$$

where ω_p is the bulk plasma frequency given by $\omega_p = \sqrt{4\pi n_0/m} = 5.89$ eV, and γ accounts for the damping.

The quantum corrected model (QCM) allows to introduce the tunneling effect into the classical Maxwell equations. We use the local approach where the nanowires are described with Drude model Eq. 4, and the tunneling across the vacuum gap between the nanowires is accounted for by filling the junction with an effective dielectric medium.³³ It is described with the Drude model, similar to Eq. 4:

$$\varepsilon_{\text{eff}}(y, S, \omega) = 1 - \frac{\omega_p^2}{\omega(\omega + i\gamma_{\text{eff}}(y, S))}. \quad (5)$$

The effective damping γ_{eff} models transition from resistive (large S) to conductive (small S) character of the junction. Thus, it acquires a dependence on the separation distance S and y -coordinate. For very large S the QCM is exactly equivalent to local classical approach. No tunneling is possible and the vacuum gap limit is retrieved with $\varepsilon_{\text{eff}}(y, S, \omega) = 1$. In this work we use exactly the same parametrization of ε_{eff} as in the earlier publication, where the QCM is introduced and described in great detail.³³

Within the non-local hydrodynamic description the transverse component of the permittivity tensor is given by Eq. (4), and the longitudinal component acquires the wave vector k dependence:

$$\varepsilon_L(\omega) = 1 - \frac{\omega_p^2}{\omega(\omega + i\gamma) - \beta^2 k^2}. \quad (6)$$

The β parameter is given by $\beta = \sqrt{3/5}v_F$.^{2,35,36,40-42} In the present case, the Fermi velocity of conduction electrons $v_F = \sqrt[3]{3\pi^2 n_0/m} = 1.05 \cdot 10^6$ m/s, resulting in $\beta = 0.81 \cdot 10^6$ m/s. Provided transverse and the longitudinal components of the permittivity tensor the absorption cross-section is calculated with numerical approach as recently implemented by G. Toscano and coworkers within the Comsol Multiphysics package.⁴²

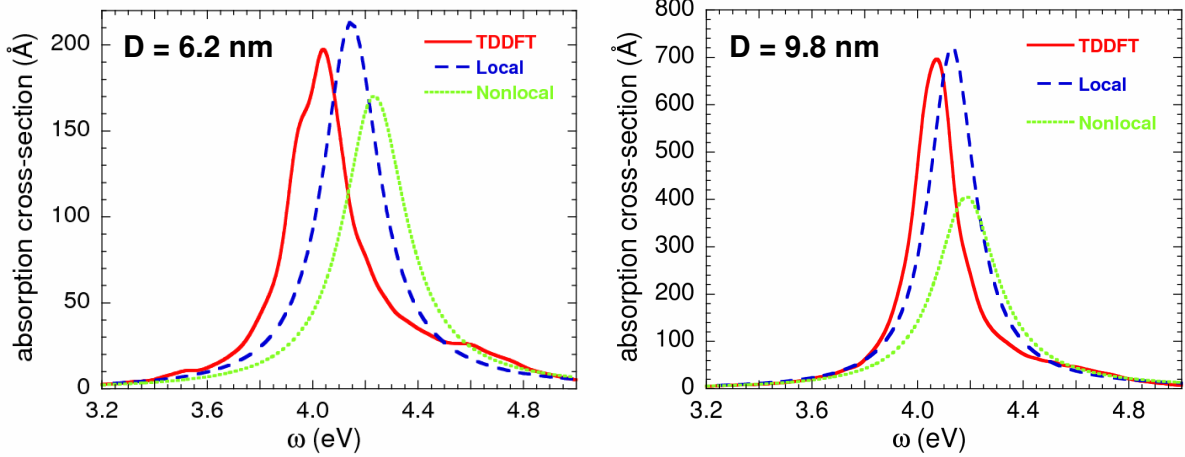


Figure 2: Absorption cross section σ for the single jellium nanowire of the diameter $D = 6.2$ nm (left) and $D = 9.8$ nm (right). Results are shown as function of the frequency ω of the incident radiation. The incoming field is the x -polarised plane wave. The TDDFT calculations are compared with results of the classical electromagnetic calculations using local (Drude) and nonlocal hydrodynamic response. (See the legend for definition of different symbols used in the figure).

Results and discussion

Individual Nanowire

We first characterize the linear optical response of individual nanowire. In Fig. 2 we show the dipole absorption cross-section σ calculated with full quantum TDDFT method and with classical local Drude and non-local hydrodynamic approaches. The classical local approach with the Drude model given by Eq. 4 for the permittivity of the nanowire leads to the dipole resonance located at surface plasmon frequency $\omega_{sp} = \omega_p/\sqrt{2} = 4.16$ eV irrespectively of the nanowire diameter. We find that the absolute value of σ and the width of the resonance as calculated with TDDFT is best reproduced with damping parameter $\gamma = 0.275$ eV for the $D = 6.2$ nm nanowire, and $\gamma = 0.247$ eV for the $D = 9.8$ nm nanowire. The smaller damping obtained for larger nanowire indicates smaller decay due to surface scattering. Indeed, the surface scattering contribution to the damping can be expressed as $\gamma_S = Av_F/R_{cl}$,⁶⁷ where $R_{cl} = D/2$ is the cylinder radius, and A is the system-dependent parameter. The calculated change of the damping is consistent with $A = 0.5$ in accord with available experimental and theoretical results for alkali clusters.^{68,69} Obviously, through the

width of the single wire resonance the quantum size effects would affect the optical response of the nanowire dimer.⁷⁰

The dipole resonance calculated with TDDFT is *red shifted* from the classical ω_{sp} value but approaches ω_{sp} for increasing size of the system. For the $D = 6.2$ nm nanowire, the resonance is at $\omega = 4.027$ eV, and it is at $\omega = 4.072$ eV for the $D = 9.8$ nm nanowire. Thus, present TDDFT results for cylindrical nanowire show the same trends as studied in detail for spherical alkali metal clusters.^{64,71–73} The non-local effect at the origin of the red shift of the plasmon resonance is linked with dynamical screening of the fields by conduction electrons. The dipole resonance frequency can be found from:^{72–75}

$$\omega/\omega_{\text{sp}} = 1 - \text{Re}[d(\omega_{\text{sp}})]/R_{\text{cl}} + O(R_{\text{cl}}^{-2}). \quad (7)$$

The real part of Feibelman’s parameter $\text{Re}[d(\omega)]$ gives the position of the centroid of the induced charge density.^{76–78} When measured from the jellium edge, $\text{Re}[d(\omega_{\text{sp}})]$ is positive for alkali metals, i.e. the screening charge is shifted into the vacuum because of the spill out of the conduction electrons outside the metal. From the calculated resonance frequency we obtain $\text{Re}[d(\omega_{\text{sp}})] = 1 \text{ \AA}$ in agreement with earlier calculations and experiment.^{73,76,77} Importantly, for the noble metals such as Au and Ag the final size effects lead to the *blue shift* of the dipole plasmon resonance.^{29,79} The difference between alkali and noble metals is the localised d-electron contribution to the total screening in the latter case.^{75,78–81} When the d-electron contribution is accounted for, $\text{Re}[d(\omega)]$ turns negative indicating that screening charge is predominantly induced inside metal.^{75,79,80}

For the small diameter nanowire $D = 6.2$ nm, finite size effects appear in the TDDFT calculations not only in the form of red shifts and line width changes, but also as clearly observable structures in the frequency dependence of the absorption cross section. These structures arise from the strong coupling of collective plasmon- and single electron-hole excitations. For large diameter nanowires, finite size effects become smaller and the plasmon resonance is much better defined. The TDDFT results also show shallow resonance in the optical absorption cross section

at $\omega = 4.6$ eV associated with a multipole plasmon (MP).^{82–84} The resonant frequency obtained with TDDFT is in good agreement with experimental data.^{82,84} The density oscillations of the MP proceed within the layer of the spilled out charge as obviously can not be captured within the local classical theory.

Finally, the green dotted lines in Fig. 2 show the absorption cross-section calculated with the classical non-local hydrodynamic model (NLHD).⁴² In contrast to the TDDFT result and experimental data on alkali clusters,^{72,73} the NLHD model predicts a blue shift of the dipole plasmon frequency from ω_{sp} value. The reason for this is that independent of the metal, the plasmon-induced charges in NLHD are localized within the layer of the thickness β/ω_p below the metal surface.⁴¹ Thus, the effective $Re[d_{NLHD}(\omega)]$ is always negative leading to the blue shift of the localised plasmon⁷⁸ in contradiction with the spill out effect known for alkali metals. However, negative $Re[d_{NLHD}(\omega)]$ inherent to NLHD description of conduction electrons and so the blue shift of the localised plasmon qualitatively coincides with full quantum result determined by the d -electron screening for the noble metals.^{75–82}

Coupled Nanowires

In Fig. 3 we show waterfall plots of the dipole absorption cross-section of the $D = 6.2$ nm and $D = 9.8$ nm nanowire dimers calculated with TDDFT. The results are presented as function of the frequency of the incident radiation for different widths S of the junction. The calculations have been performed for both positive and negative S , where the latter means a geometrical overlap of the nanowires. The $S = 0$ case corresponds to the kissing cylinders^{40,41} with touching jellium edges where the distance between the topmost atomic planes equals to the interlayer spacing, i.e. a continuous solid is formed at the contact point.

For large positive separations the non-local effects including electron tunneling across the junction are small, and the TDDFT results agree with earlier classical calculations^{41,41,47,58,59} (See also Fig. 5). At $S = 26.5$ Å the absorption spectrum is dominated by two resonant structures. First is the bonding dipole plasmon (DP) indicated with blue dotted line in Figure. It is formed from

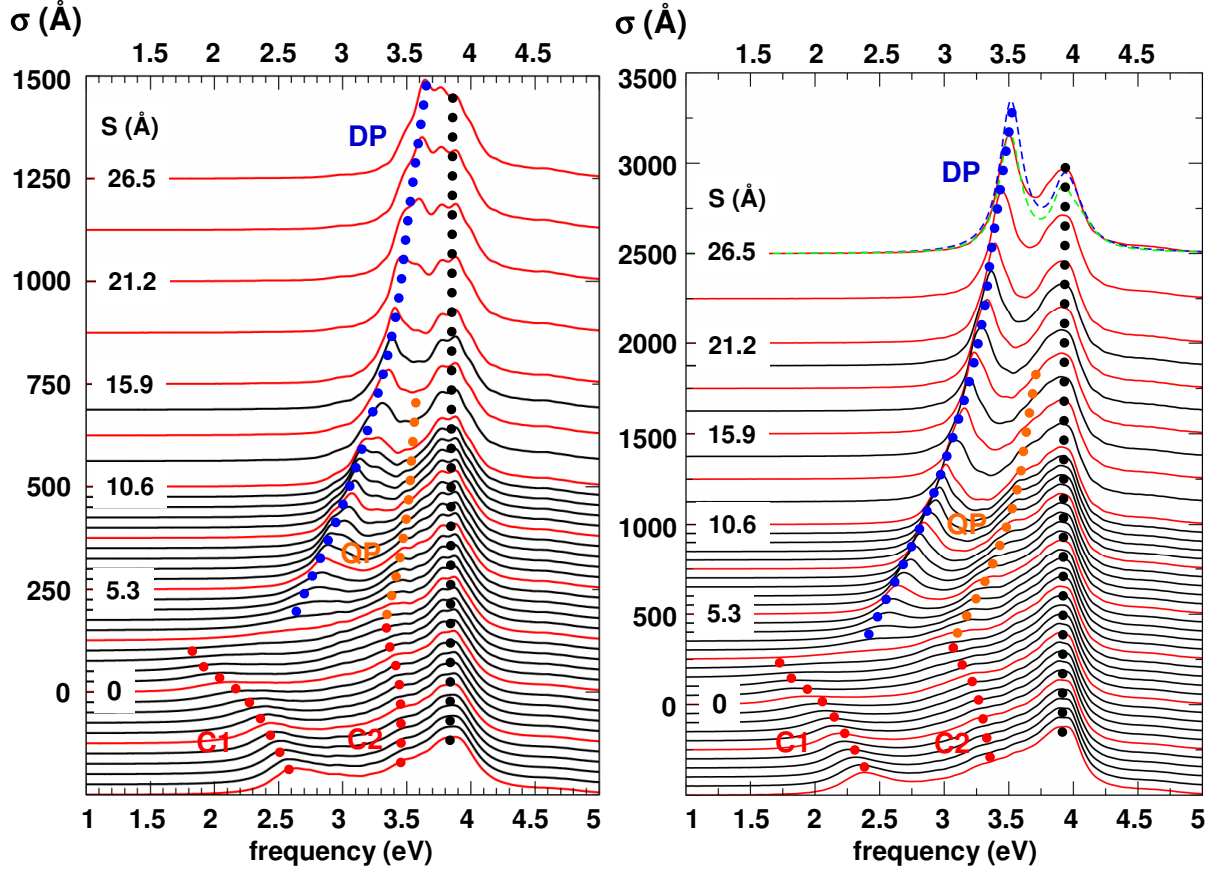


Figure 3: Waterfall plot of the dipole absorption cross-section for the nanowire dimer in vacuum. The dimer consists of two Na nanowires of diameter $D = 6.2$ nm (left) and $D = 9.8$ nm (right) separated by variable distance S . The incoming field is the x -polarised plane wave. The centers of the particles are at $x = \pm(D + S)/2$, and S is negative for overlapping cylinders. $S = -D$ would correspond to the limit of a single cylinder. TDDFT results are given as function of the frequency ω of the incident radiation for different separations S . For clarity a vertical shift proportional to the separation distance is introduced for each absorption spectrum. The red curves are used each $5 a_0 \approx 2.65$ Å of S -change. These are labeled with corresponding S -values each $10 a_0 \approx 5.3$ Å of S -change. The plasmonic modes responsible for the peaks in the absorption cross-section are labelled. DP stands for the Bonding Dipole Plasmon, QP for Bonding Quadrupole Plasmon, and C1 for the lowest (dipole) Charge Transfer Plasmon, C2 for the higher energy Charge Transfer Plasmon. Vertical black dotted line shows the degenerate plasmon peak located close to ω_{sp} . On the right panel the blue (green) dotted curve at $S = 26.5$ Å shows results of the classical Drude (NLHD) calculations with adjusted parameters. Further details are give in the main text of the paper.

hybridization of the dipole plasmon modes of the individual nanowires. The second resonance indicated with black dotted line is formed by bonding quadrupole (QP) plasmon degenerated with higher order modes. It is slightly red shifted with respect to the surface plasmon frequency ω_{sp} . At $S \rightarrow \infty$, the DP merges into the degenerate mode and the spectrum evolves into that of the individual nanowire. As the junction width S decreases, the DP shifts to lower frequencies because of the attractive interaction between the charges of opposite sign across the junction. Along with red shift of the DP, the QP (orange dotted line in Figure) splits from the degenerate mode, and shows the red shift with decreasing S .

Despite the overall similarity of the results obtained with smaller and larger diameter nanowires there are some notable differences primarily caused by finite size effect. The resonances are much better defined for the larger $D = 9.8$ nm nanowire. In this case the width of the resonances is smaller and the structures due to the interaction between the plasmon and electron-hole pair excitations disappear. For $D = 6.2$ nm nanowire, this interaction can even split the single plasmon peak into several lines. The red shift of the DP and QP modes with decreasing S is more pronounced for the $D = 9.8$ nm nanowire dimer. This is because of the scale (S/D) invariance of the plasmonic properties of nanostructure in the quasistatic limit.

For junction widths below ~ 7 Å, electron tunneling across the junction becomes important. The results obtained here for the nanowire dimer have much in common with those reported in quantum studies of touching spherical nanospheres,^{31–33} and in recent experiments.^{28,29} The DP resonance progressively disappears and the charge transfer plasmon mode (C1) emerges prior to the direct contact between the nanoparticles. C1 appears as a broad shallow low-frequency peak at positive $S \simeq 1.5$ Å, and evolves into a well-defined resonance at $S < 0$. Similarly, because of electron tunneling, the QP mode continuously evolves into a higher order charge transfer plasmon mode C2 before direct contact between the nanowires. Thus, already at positive S the nanowires appear conductively connected showing characteristic charge transfer plasmon modes.^{45,48–51} For a dimer with well established conductive contact, the C1 and C2 modes experience a blue shift as also reported in classical calculations.^{45,63}

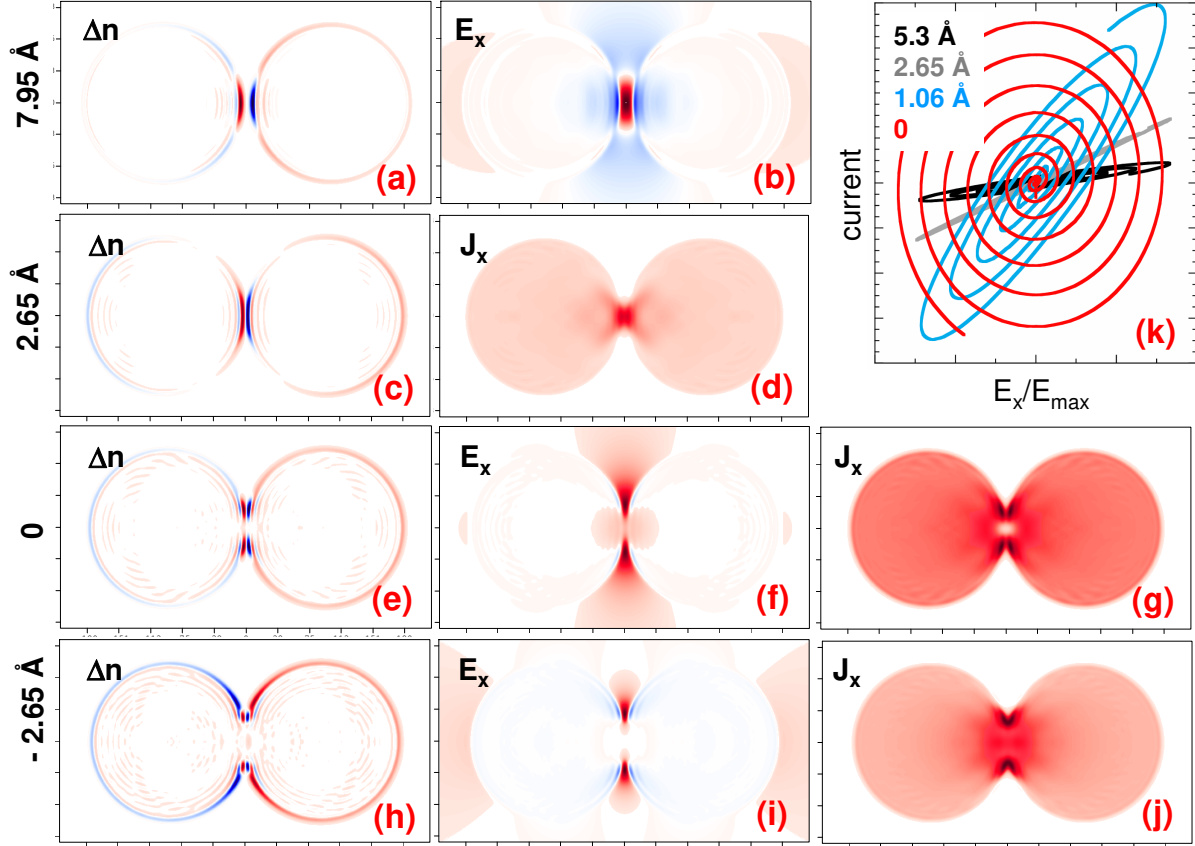


Figure 4: Panels (a)-(k) Detailed analysis of the plasmon dynamics in the coupled Na nanowires of diameter $D = 9.8$ nm. The incident x -polarised laser pulse is at resonance with lowest (dipole plasmon mode of the system). Panels (a)-(j) present the snapshots of the induced charge density Δn , current density J_x , and field E_x for different junction widths S as indicated to the left of each row. The induced currents and fields are measured along interparticle x -axis. Positive (negative) values correspond to red (blue) color code. The induced densities are shown at the instant of time corresponding to the maximum dipole moment of the dimer. The induced currents and fields are shown at the instants of time when the induced fields in the junction reach maximum. Panel (k): Conductivity analysis. The current J_x measured on x -axis in the middle of the junction is plotted as a function of the normalized electric field at the same position. Different colors correspond to different separations S as explained in the insert.

To obtain further insights into the effect of the tunneling through the junction we have calculated the electron density dynamics in the plasmonic dimer subjected to an incident x -polarized laser pulse resonant with lower (DP or C1) plasmonic modes. The panels (a)–(j) of Fig. 4 show snapshots of the induced charge density Δn , and x -component of the current density J_x , and field E_x for different junction widths S . Results are given for the case of $D = 9.8$ nm nanowires. The induced densities are shown at the instant of time corresponding to the maximum dipole moment of the dimer. The currents and fields are shown at the instant of time corresponding to the maximum induced field in the junction.

For large separation $S = 7.95$ Å the maximum induced dipole corresponds to the in-phase dipole polarisation of each nanocylinder expected for the DP mode. High charge densities are induced at the surfaces facing the junction resulting in large electric field enhancement $|E_0/E_{in}| \sim 80$. Here, E_{in} is the amplitude of the incident field and E_0 is the amplitude of the field measured at the x -axis in the middle of the junction. The structure of the induced charges and fields are similar to previous classical results for coupled cylinders^{41,47,58,59} and also resembles much to the case of metal sphere dimer.⁴⁵ The probability of tunnelling between nanowires is negligible and no current flows across the junction. Note that the maximum dipole polarisation corresponds to the instant of time when the maximum charge separation has occurred and the currents inside nanoparticles are minimal. For the reduced width $S = 2.65$ Å, very similar profiles for induced densities and fields are obtained. Therefore, we do not show E_x but focus on the induced current. The junction width is now sufficiently small to allow weak electron tunnelling between the nanoparticles. Large optical field in the junction acts as large BIAS in the scanning tunneling microscope causing tunneling current across the junction.³³ Thus, the junction shows the *resistive* character with maximum current between nanowires reached at the maximum field and consequently at maximum induced dipole.

Further reduction of the separation S increases the tunneling probability and short circuits the junction. When conductive contact is formed, the DP mode disappears and the C1 mode emerges in the absorption spectrum. Panels (e) and (h) Fig. 4 show the induced charges for $S = 0$ and $S = -2.65$ Å, respectively. The results are very similar, i.e. already for the $S = 0$ case of kissing

cylinders the charge transfer plasmon mode is well developed (see also Fig. 3, and Fig. 5). The maximum dipole moment of the dimer corresponds to the oppositely charged nanowires. Maximum currents and fields [panels (f), (g), (i), (j)] are reached when the total dipole moment of the system is minimum (compare with $S = 2.65 \text{ \AA}$ case). Precisely, this is large current flowing through the entire system that builds the dipole polarisation with opposite charges at left and right nanowires consistent with resonant excitation of the C1 mode. The field enhancement is about 30 for both $S = 0$ and $S = -2.65 \text{ \AA}$ separations. However, the fields are screened at the center of the junction, and the maximum fields are located at its sides. This is similar to the classical result for the overlapping cylinders.⁶³

Panel (k) of Fig. 4 provides further analysis for the evolution from resistive to conductive character of the junction with decreasing S . The current $J_x(t)$ on the x -axis at the middle of the junction between the nanowires is shown as a function of the field $E_x(t)$ at the same location. At large separations, the linear relation $J_x(t) = gE_x(t)$ between the current and the local field shows that the junction is resistive. The increase of the slope g when S is reduced from $S = 5.3 \text{ \AA}$ to $S = 2.65 \text{ \AA}$ is because of the increase of the tunneling probability. For $S = 1.06 \text{ \AA}$ and $S = 0 \text{ \AA}$ the $E_x(t)$ and $J_x(t)$ acquire a relative phase. Since the field envelope of the incident pulse grows in time for the time interval shown in Fig. 4(k), the clock-wise rotation of the $J_x(t)[E_x(t)]$ curve implies that the current is retarded with respect to the field. The junction becomes conductive which is particularly apparent for $S = 0$.

The TDDFT results show that for small junction widths the optical response is determined by electron tunneling. For large width of the junction the tunneling is negligible. Each cylinder responds on the self consistent field created by the incident radiation and the neighbour. The effects of nonlocal screening discussed for the single cylinder should *a priori* influence the optical response of the dimer as suggested with NLHD calculations⁴⁰⁻⁴³ and as inherently build in the TDDFT results. While the effect of tunneling is clearly seen with TDDFT calculations, revealing the role of the nonlocal screening requires comparison with classical results, in particular for the energies of the plasmonic modes. In this respect, present system offers a unique opportunity to test

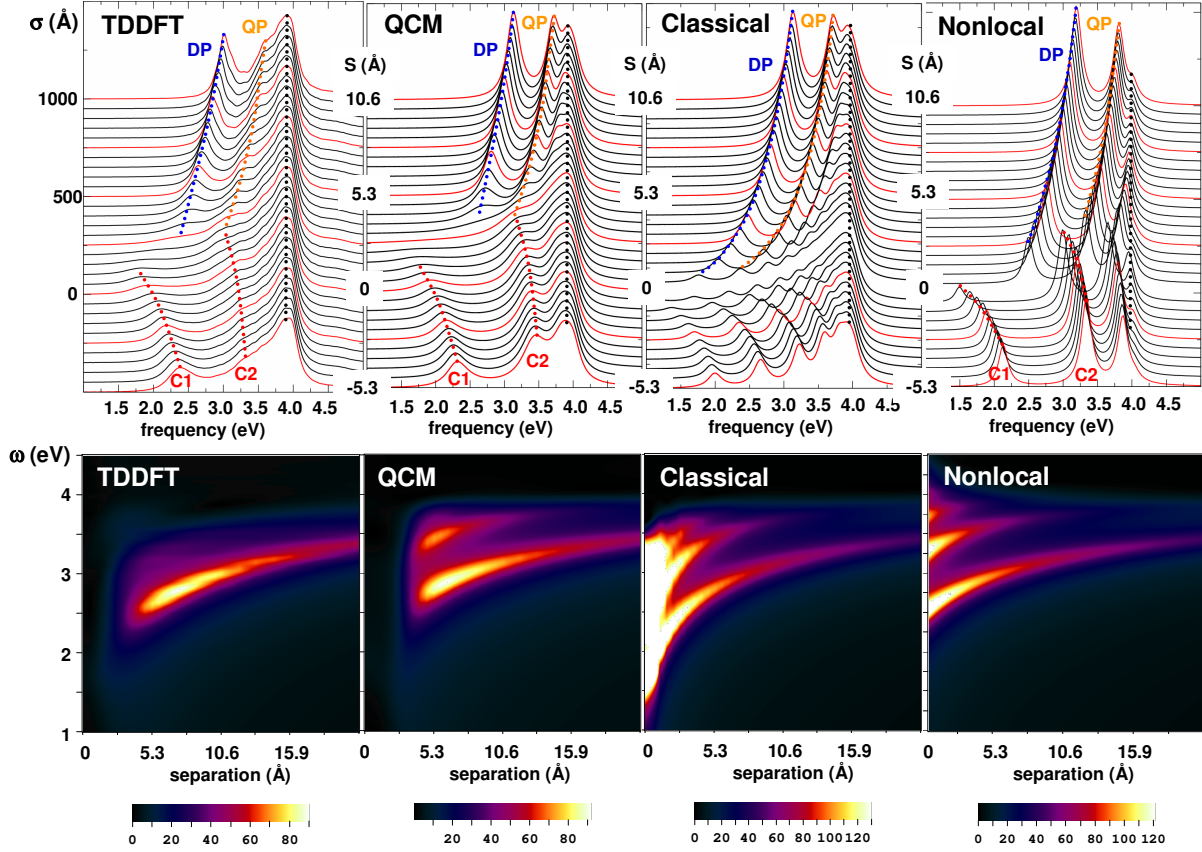


Figure 5: Comparison of the optical properties of a nanowire dimer obtained with the full TDDFT calculations, with the quantum corrected model (QCM), with a classical Drude electromagnetic calculations (Classical), and with calculations based on the nonlocal hydrodynamic model (Nonlocal). The dimer consists of two $D = 9.8$ nm Na nanowires in vacuum. The incoming plane wave is polarized along the dimer axis x . Upper panels: Waterfall plots of the dipole absorption cross-section as function of the width of the junction S . Red curves correspond to separation distances of $S = -5.3$ Å, -2.65 Å, 0 Å, 2.65 Å, 5.3 Å, 7.95 Å, and 10.6 Å. For further details see caption of Fig.3 Lower panels: Color plots of the local field enhancement at the center of the junction for positive separations. Results are shown as function of the frequency ω of the incident radiation and separation distance S . The color code is explained at the bottom of the corresponding panels.

the validity of different classical models against full quantum results for relatively large system, with fully developed plasmonic modes, and with dielectric properties well described within free electron approximation. The rest of the paper is devoted to quantum vs classical comparison with particular focus on possibility to account for quantum effects within classical approach.

Quantum vs classical approaches

Fig. 5 shows the present TDDFT results, the QCM results, results from classical calculations based on the Drude description of Na dielectric function, and results of the NLHD calculations. Waterfall plots of the absorption cross-section (upper panels) and contour plots of the field enhancement on the x -axis at the middle of the junction are presented as function of the frequency of the incoming plane wave and of the junction width S . Since for the individual nanowire TDDFT gives a red shift of the dipole plasmon resonance from the classical ω_{sp} position, while NLHD leads to a blue shift (Fig. 2), we adjust the parameters of different models. For the sake of comparison of the junction width dependence we enforce an agreement between the TDDFT, QCM, classical Drude, and NLHD at the largest S calculated here with TDDFT, $S = 26.5 \text{ \AA}$ (see Fig. 3). For the $D = 9.8 \text{ nm}$ nanowire dimer we have used plasma frequency $\omega_p = 5.8 \text{ eV}$ and damping $\gamma = 0.247 \text{ eV}$ in the QCM and classical Drude calculations. Thus, only small correction to the bulk plasma frequency (nominal value 5.89 eV) is required in this case. The NLHD model needs for much larger correction to compensate for the blue shift inherent to this treatment. We used $\omega_p = 5.5 \text{ eV}$ and $\gamma = 0.16 \text{ eV}$. Adjustment of the nonlocality parameter β is also possible, but then the model loses its predictive power. Indeed, as far adjustment is limited to ω_p and γ parameters, the finite size effects and so the need for correction will disappear with increasing size of the nanoobjects.

The main features of the quantum results have been discussed in connection with Fig. 3 so here we will focus on comparisons between different model approaches. As follows from Fig. 5, the QCM does an excellent job in describing the TDDFT results over the entire range of separations S addressed here. The important features such as: the number of resonances; their distance dependence; the transition from the separated to conductively coupled regime are well reproduced.

In particular, in sheer contrast with classical theory^{41,45,47,58,59} the change of the spectrum at the moment of contact is progressive and fields at the middle of the junction are quenched, not diverging with decreasing junction size. Besides qualitative aspects, we find that the TDDFT and QCM agree semi-quantitatively as is further stressed in Fig. 6. This figure zooms into the most delicate interaction regime corresponding to the transition from the separate to overlapping nanowires.

By construction of QCM, it is equivalent to the classical local Drude description for large positive S where tunneling is negligible. The good agreement with TDDFT data suggests that the pure local classical description is reasonable for a large S . At the same time the classical description fails at small $S \sim 5 \text{ \AA}$, i.e. typically at two lattice constants between surface atomic planes that define the junction.²⁹ The accumulation of charges on the opposite sides of the junction leads to exaggerated coupling between nanowires resulting in diverging fields and too large number of resonances. Similarly, for negative S , the sharp edges of the junction, which are otherwise smeared out by the electron tunneling also result in too many hybridized resonances.³³

The NLHD description is free from the $S = 0$ divergence problem.^{40,41} The number of resonances remains small and the fields in the middle of the junction stay finite albeit too large. This can be easily understood thanks to the elegant transformation optics approach developed for interacting cylinders by Fernández-Domínguez and coworkers.⁴¹ At positive S an analytic solution is found which depends on the renormalised parameter $\tilde{S} \simeq S + 2\delta$, where $\delta \simeq \beta/\omega_p$ (1 \AA in the present case). The physics behind this shift is the localisation of the plasmon-induced charge below the surface as inherent for the NLHD model. As we discussed for the single cylinder, in terms of the dynamical screening theory, δ is equivalent to an effective Feibelman parameter $\delta = -\text{Re}[d_{\text{NLHD}}(\omega)]$. Thus, even for $S = 0$, the induced charges at the opposite sides of the junction are actually separated by a finite distance 2δ . However, since the tunneling is not accounted for, the NLHD description fails to reproduce the quenching of the field enhancement at the middle of the junction for small positive S . The NLHD also fails to smoothen out the transition from separated to overlapping regimes and gives an abrupt nonphysical transition. The number of modes is smaller than in the classical Drude description, but still larger than what is obtained in TDDFT or

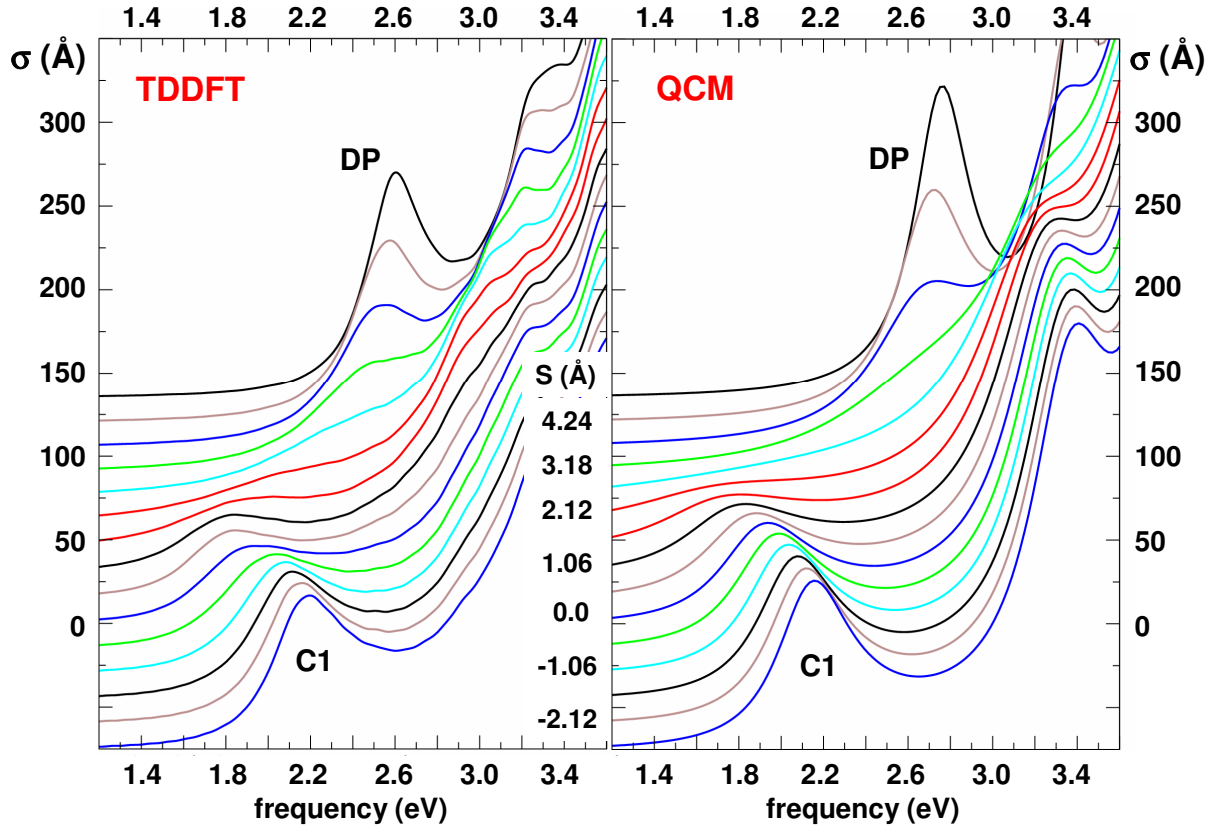


Figure 6: Detailed comparison between TDDFT and QCM calculations. The dipole absorption cross-section of the $D = 9.8$ nm Na nanowire dimer is shown for small separations S corresponding to the strong tunneling regime and transition from separated to conductively coupled nanowires. The frequency range is zoomed at the transition from the bonding dipole (DP) to the lowest charge transfer (C1) plasmon. Waterfall plots of the optical absorption cross-section are shown for the separation distances changing from $S = -2.65$ Å (lowest blue line) to $S = 4.77$ Å (upper black line) in steps of $1 a_0$ (0.53 Å). For further details see caption of Fig. 3.

QCM calculations.

Our final remark concerns the QP plasmon that evolves into the C2 charge transfer mode for negative S . The associated resonances are much less pronounced in the TDDFT cross-section compared to model approaches. One possible reason is finite size effect, where the system size is not large enough for the corresponding density oscillations to be completely formed. However, the similarity between the TDDFT results for $D = 6.2$ nm and $D = 9.8$ nm nanowire dimers as shown in Fig. 3 suggests that this quantum size effect is small. We thus tentatively attribute the weaker high order resonances as obtained in TDDFT to the effect of the smearing of the induced surface charge densities. This *a priori* reduces the coupling between the dipole and higher order modes and consequently the intensity of the QP resonance in the dipole absorption cross-section.

Dynamic screening

With results shown in the previous Subsection, tunneling determines the optical properties of the system at small junction widths. For large width S tunneling is absent and nonlocal dynamic screening influences the optical properties. Similar to the case of the individual nanowire, the major nonlocal effect is the red shift of the frequency of the bonding dipole plasmon as compared to the classical prediction. However, for the dimer, this effect is much stronger, and does not disappear with increasing radius of nanoparticle.

Fig. 7 presents the analysis of the role played by dynamic screening in determining the frequency of the bonding dipole plasmon. Panel (a) gives schematic representation of the location of plasmon induced screening charges in the junction of width S . Within the local classical approach the screening charges are localised at geometrical surfaces of the cylinders separated by S . We recall that we use the definition of the geometrical surface such that it coincides with jellium edge. Within TDDFT, the real part of the centroid of the induced charge density $Re[d(\omega)]$ corresponds to the position of the plasmon-induced surface charges with respect to the jellium edge of each cylinder.^{74–78,80,82} For the present case of sodium nanowires, $Re[d(\omega)]$ is positive ≈ 0.9 Å in the frequency range of interest.⁷⁷ This means that the screening charge is shifted by 0.9 Å into

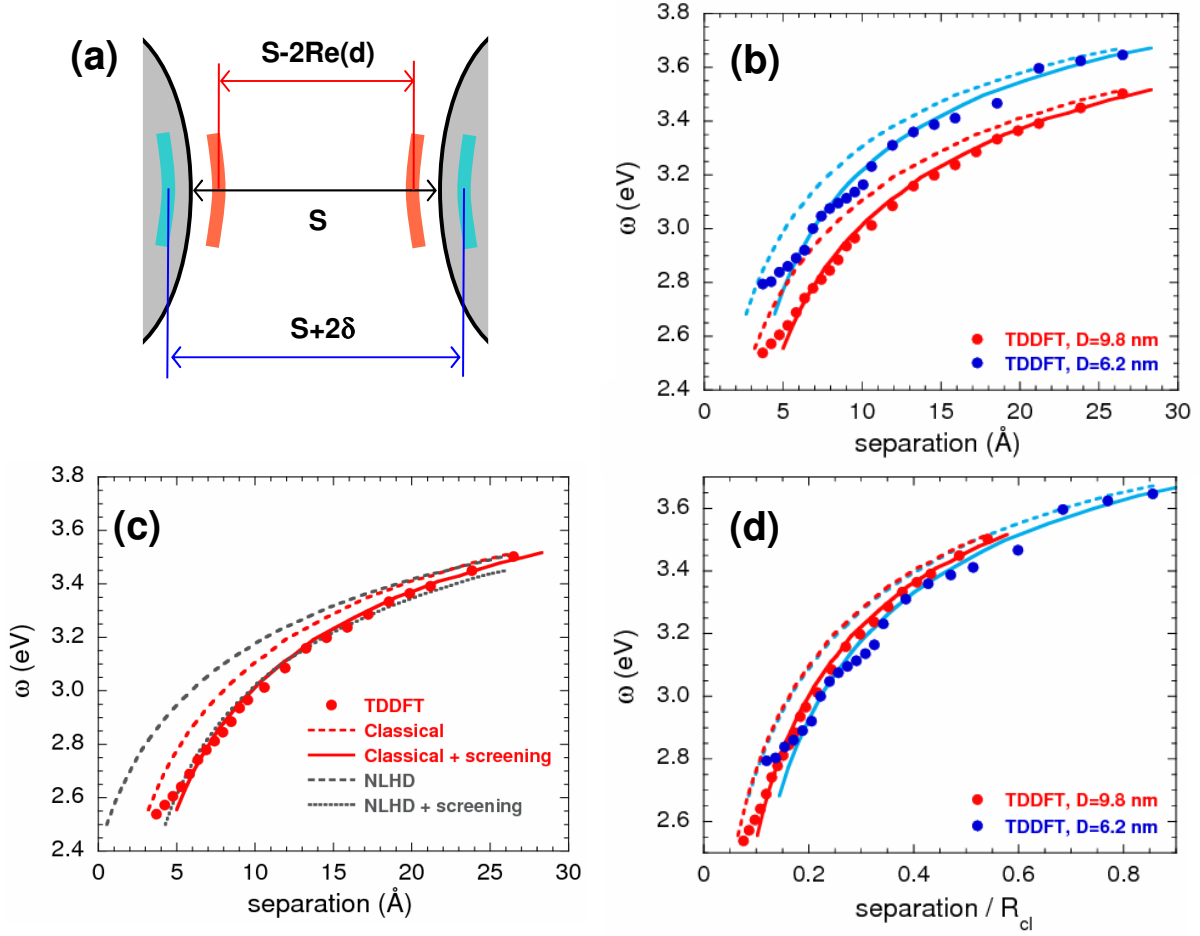


Figure 7: Dynamic screening. (a) Schematic representation of the location of plasmon induced screening charges in the junction. Within the local classical approach the screening charges are at geometrical surfaces of the cylinders (here equivalent to the jellium edges) separated by the junction of width S . Within the TDDFT, the centroids of the screening charges (red areas) are located at $\text{Re}[d(\omega)]$ in front of the jellium edges and separated by $S - 2\text{Re}[d(\omega)]$. In NLHD approach the centroids of the screening charges (blue areas) are located at distance δ below the geometrical surface and separated by $S + 2\delta$. (b) Energy of the dipole plasmon resonance as function of the junction width S . Dots: TDDFT results obtained for nanowire dimers formed by $D = 6.2$ nm and $D = 9.8$ nm nanowires (see the legend). Solid and dashed lines show results of classical Drude calculations for $D = 6.2$ nm (blue) and $D = 9.8$ nm (red) dimers. Dashed lines: separation S is measured between the jellium edges. Solid lines: separation S is measured between the centroids of the induced charges. For more details see the main text. (c) Energy of the dipole plasmon resonance as function of the junction width S . Dots: TDDFT results obtained for $D = 9.8$ nm nanowire dimer. Solid and dashed red lines show results of classical Drude calculations [same as (b)]. Dashed and dotted gray lines show results of NLHD calculations. Dashed line: separation S is measured between the jellium edges. Dotted line: separation S is measured between the centroids of the induced charges. (d) Same as (b), but results are shown as function of the scaled separation S/R_{cl} , where $R_{cl} = D/2$ is the nanowire radius.

the vacuum and located at $\approx 3 \text{ \AA}$ outside the surface atomic plane of the nanoparticle. The distance between the plasmon induced charges across the junction is thus $\Sigma = S - 2\text{Re}[d(\omega)]$. As to the NLHD approach, with present choice of the non-locality parameter β it places the screening charges at $\delta = 1 \text{ \AA}$ inside the geometrical surface. Thus, within the NLHD approach the screening charges are separated by the distance $S + 2\delta$.

This insight provides an explanation for the junction width dependence of the DP modes shown in Fig. 7(b) for two different nanowire dimers. While the overall agreement between the classical Drude (dashed lines) and the TDDFT (dots) calculations is good, the TDDFT result is systematically redshifted. The difference is increasing with decreasing S indicating that the classical calculations underestimate the coupling between the dipole plasmons localized on each nanowire. Our finding that the plasmon-induced charges in the TDDFT calculations are outside the nanoparticle surfaces explains this effect. Indeed, the actual energy of the DP is given by the interaction between the screening charges across the junction. Thus, the TDDFT data obtained for junction width S should be compared with classical results calculated for $\Sigma = S - 2\text{Re}[d(\omega)]$. If the DP dispersion is plotted as a function of effective junction width given by the distance between plasmon induced screening charges, the agreement between TDDFT and the classical simulations becomes excellent. We note in passing that the step-structure of the TDDFT data for the smaller $D = 6.2 \text{ nm}$ dimer stems from the strong coupling between plasmon and electron-hole pair excitations.

A similar analysis can be performed for the NLHD model calculations shown in Fig. 7(c) for the case of $D = 9.8 \text{ nm}$ nanowire dimer. The NLHD results appear at even higher frequencies than the classical Drude calculations, in even stronger disagreement with the TDDFT than the classical model. The explanation for this is that NLHD artificially places the plasmon-induced screening charges at a position $\sim \delta = 1 \text{ \AA}$ inside the metal surface. Thus, the separation between screening charges $S + 2\delta$ in the NLHD model is larger than separation S in pure local theory, and too large compared to the quantum result $\Sigma = S - 2\text{Re}[d(\omega)]$. This decreases the interaction and results in blue shifted DP modes compared to the classical model and TDDFT. If the DP dispersion is plotted as a function of effective junction width, agreement between NLHD, classical Drude, and TDDFT

results is obtained.

The above results show that the TDDFT dispersion of the DP can be fully retrieved with local classical calculations. The main issue here is the size of the junction for which the calculations have to be performed. For geometry of the nanostructure, it seems convenient to define the surfaces of the objects as given by the jellium edges. In this case the width $S = 0$ of the junction would correspond to continuous solid formed at the contact point, which is physically sound. On the other hand, classical calculations have to be performed for the effective junction width given by the actual separation between the screening charges. These conclusions have direct implications for the ultimate limit of resolution of plasmonic rulers.¹⁸

For the free-electron Na surface, the screening charges are located at approximately 0.9 \AA (3 \AA) outside the jellium edge (surface atomic layer) meaning that for a Na–Na junction, the effective junction width would be 1.8 \AA (6 \AA) smaller than the physical junction width measured between the jellium edges (surface atomic planes). This conclusion holds not only for the nanowire case considered here, but for any junctions between Na surfaces. For silver and gold, analysis of the data on the blue shift of the dipole plasmon resonance in small clusters^{29,75,79,85,86} with Eq. 7 places the effective screening charges inside the jellium edge at $1.5 \div 0.85 \text{ \AA}$ for silver, and at approximately 1.5 \AA for gold. Therefore, for an Ag–Ag (Au–Au) junctions, the effective junction width would be by $1.7 \div 3 \text{ \AA}$ ($\sim 3 \text{ \AA}$) larger than the physical junction width measured between the jellium edges and close to the junction width measured between the surface atomic planes.

The use of the plasmon ruler relies on the universal dependence of the DP frequency on the scaled separation.^{16,17} In Fig. 7(d) we show the TDDFT and classical results for the DP frequency of the $D = 6.2 \text{ nm}$ and $D = 9.8 \text{ nm}$ nanowire dimers as function of the scaled separation S/R_{cl} . The TDDFT data for both nanowire dimer sizes nearly falls on the unique curve provided that the separations S are sufficiently large that no tunneling occurs. This holds for S larger than typically 2 lattice constants between surface atomic planes, which sets lower bound for the distances that can be actually measured with plasmon ruler.

Summary and Conclusions

In conclusion, we have presented fully quantum mechanical study of the optical response of the plasmonic dimer formed by realistic size cylindrical nanowires. This system is also representative of interacting nanorods and is of relevance for SERS, plasmon ruler, and plasmon transport applications. Translational invariance allows to apply the time-dependent density functional theory for the plasmonic dimer of largest size considered so far in quantum calculations.

We considered nanowires made of Sodium which is a prototype for free-electron metal so that jellium model applies. The free-electron character of Na valence electrons implies that its permittivity can be well described with Drude model, as well as it is consistent with approximations behind the hydrodynamic approach to model the nonlocal character of the dielectric function. Thus, this is the system of choice allowing to set the full quantum TDDFT benchmark results, and to use these results to test different theoretical approaches addressing plasmonic response of the strongly coupled objects. This was one of the central goals of the present work.

We have found that for the small junction widths, the optical response is determined by the quantum tunneling of conduction electrons across the potential barrier separating the nanowires. A decreasing junction size leads to progressive attenuation of the plasmon modes of separated nanowires and the emergence of charge transfer plasmon modes of conductively coupled dimer. As this happens, the fields in the middle of the junction are screened. The maximal field enhancement moves from the middle to the external regions of the junction. In this distance range the classical local Drude and nonlocal hydrodynamic model descriptions fail since they do not account for tunnelling. At variance, the quantum corrected model reproduces the TDDFT findings on a semi-quantitative level.

For large separations S , the tunneling is negligible and the overall agreement between TDDFT, classical and the QCM results is good. Thus the QCM performs well over the entire range of separations studied here. For large S the agreement between the classical and TDDFT results can be further improved by taking into account the shift of the plasmon-induced charge density with respect to the geometrical surface of the nanoparticle. The latter can be defined as the jellium edge

as in the present work, or as the top most atomic layer at the surface. The effective junction width is then given by the separation of plasmon induced charges at the opposite sides of the junction. Indeed, this is the interaction between these charges that determines the hybridization and energies of the modes. Introducing a simple distance correction into the classical calculations allows a full account of this non-local effect. This result has implications for the plasmon ruler concept and shows that care should be taken with respect to the definition of the separation which is actually measured.

We hope that the results presented here contribute to the understanding of the role of quantum nonlocal effects in strongly coupled plasmonic systems, and help in elaborating efficient theoretical approaches for their prediction.

ACKNOWLEDGEMENTS We thank Guiseppe Toscano for providing NPL extension to Comsol 4.2a RF Module used in our nonlocal calculations as well as for his kind assistance. J.A. acknowledges financial support from the Department of Industry of the Basque Government through the ETORTEK project nanoiker, the Spanish Ministerio de Ciencia e Innovación through Project No. FIS2010-19609-C02-01 and Project No. EUI2008-03816 CUBIHOLE from the Internationalization Program. P.N. Acknowledges support from the Robert A. Welch Foundation (C-1222) and the Office of Naval Research (N00014-10-1-0989).

References

- (1) Kelly, L.; Coronado, E.; Zhao, L. L.; and Schatz, G. C. The Optical Properties of Metal Nanoparticles: The Influence of Size, Shape and Dielectric Environment. *J. Phys. Chem. B* **2003**, 107, 668.
- (2) Alvarez-Puebla, R.; Liz-Marzán, L. M.; and García de Abajo, F. J. Light Concentration at the Nanometer Scale. *J. Phys. Chem. Lett.* **2010**, 1, 2428.

- (3) Schuller, J. A.; Barnard, E. S.; Cai, W.; Jun, Y. C.; White, J. S.; and Brongersma M. L. Plasmonics for extreme light concentration and manipulation. *Nature Materials* **2010**, 9, 193.
- (4) Halas, N. J.; Lal, S.; Chang, W.-S.; Link, S.; and Nordlander, P. Plasmons in Strongly Coupled Metallic Nanostructures. *Chem. Rev.* **2011**, 111, 3913.
- (5) Pasquale, A. J.; Reinhard, B. M.; Negro, L. D. Engineering Photonic-Plasmonic Coupling in Metal Nanoparticle Necklaces. *ACS Nano* **2011**, 5, 6578.
- (6) Xu, H.; Bjeneld, E.; Käll, M.; Börjesson, L. Spectroscopy of Single Hemoglobin Molecules by Surface Enhanced Raman Scattering, *Phys. Rev. Lett.* **1999**, 83, 4357.
- (7) Talley, C. E.; Jackson, J. B.; Oubre, C.; Grady, N. K.; Hollars, C. W.; Lane, S. M.; Huser, T. R.; Nordlander, P.; Halas, N. J. Surface-Enhanced Raman Scattering from Individual Au Nanoparticles and Nanoparticle Dimer Substrates. *Nano Lett.* **2005**, 5, 1569.
- (8) Theiss, J.; Pavaskar, P.; Echternach, P. M.; Muller, R. E.; Cronin, S. B. Plasmonic Nanoparticle Arrays with Nanometer Separation for High-Performance SERS Substrates. *Nano Lett.* **2010**, 10, 2749.
- (9) Fazio, B.; D'Andrea, C.; Bonaccorso, F.; Irrera, A.; Calogero, G.; Vasi, C.; Gucciardi, P. G.; Allegrini, M.; Toma, A.; Chiappe, D.; Martella, C.; de Mongeot, F. B. Re-radiation Enhancement in Polarized Surface-Enhanced Resonant Raman Scattering of Randomly Oriented Molecules on Self-Organized Gold Nanowires. *ACS Nano* **2011**, 5, 5945.
- (10) Mühlischlegel, P.; Eisler, H.-J.; Martin, O. J. F.; Hecht, B.; and Pohl, D. W. Resonant optical antennas. *Science* **2005**, 308, 1607 (2005).
- (11) Bharadwaj, P.; Deutsch, B.; and Novotny, L. Optical antennas. *Adv. Opt. Photon.* **2009**, 1, 438.
- (12) Taminiau, T. H.; Stefani, F. D.; Segerink, F. B.; and van Hulst, N. F. Optical antennas direct single-molecule emission. *Nature Photonics* **2008**, 2, 234.

- (13) Kim, S.; Jin, J.; Kim, Y.-J.; Park, I.-Y.; Kim, Y.; and Kim, S.-W. High-harmonic generation by resonant plasmon field enhancement. *Nature* **2008**, 453, 757.
- (14) Quinten, M.; Leitner, A.; Krenn, J. R.; and Aussenegg, F. R. Electromagnetic energy transport via linear chains of silver nanoparticles. *Opt. Lett.* **1998**, 23, 1331.
- (15) Maier, S. A.; Kik, P. G.; Atwater, H. A.; Meltzer, S.; Harel, E.; Koel, B. E.; Requicha, A. A. G. Local detection of electromagnetic energy transport below the diffraction limit in metal nanoparticle plasmon waveguides. *Nature Materials* **2003**, 2, 229.
- (16) Gunnarsson, L.; Rindzevicius, T.; Prikulis, J.; Kasemo, B.; Käll, M.; Zou, S.; Schatz, G. C. Confined Plasmons in Nanofabricated Single Silver Particle Pairs: Experimental Observations of Strong Interparticle Interactions. *J. Phys. Chem. B* **2005**, 109, 1079.
- (17) Jain, P. K.; Huang, W.; El-Sayed, M. A. On the Universal Scaling Behavior of the Distance Decay of Plasmon Coupling in Metal Nanoparticle Pairs: A Plasmon Ruler Equation. *Nano Lett.* **2007**, 7, 2080.
- (18) Hill, R. T.; Mock, J. J.; Hucknall, A.; Wolter, S. D.; Jokerst, N. M.; Smith, D. R.; and Chilkoti, A. Plasmon Ruler with Angstrom Length Resolution *ACS Nano* **2012**, 6, 9237.
- (19) Ben X., Park H. S. Size-Dependent Validity Bounds on the Universal Plasmon Ruler for Metal Nanostructure Dimers. *J. Phys. Chem. C* **2012**, 116, 18944.
- (20) Liu, N.; Hentschel, M.; Weiss, T.; Alivisatos, A. P.; Giessen, H. Three-Dimensional Plasmon Rulers. *Science* **2011**, 332, 1407.
- (21) Aćimović, S. S.; Kreuzer, M. P.; González, M. U.; and Quidant R. Plasmon Near-Field Coupling in Metal Dimers as a Step toward Single-Molecule Sensing. *ACS Nano* **2009**, 3, 1231.
- (22) Juluri, B. K.; Chaturvedi, N.; Hao, Q. Z.; Lu, M. Q.; Velegol, D.; Jensen, L.; Huang, T. J. Scalable Manufacturing of Plasmonic Nanodisk Dimers and Cusp Nanostructures Using Salting-out Quenching Method and Colloidal Lithography. *ACS Nano* **2011**, 5, 5838.

- (23) Arielly, R.; Ofarim, A.; Noy, G.; and Selzer, Y. Accurate Determination of Plasmonic Fields in Molecular Junctions by Current Rectification at Optical Frequencies. *Nano Lett.* **2011**, 11, 2968.
- (24) Kern, J.; Großmann, S.; Tarakina, N. V.; Häckel, T.; Emmerling, M.; Kamp, M.; Huang, J.-S.; Biagioni, P.; Prangma, J. C.; and Hecht B. Atomic-Scale Confinement of Resonant Optical Fields. *Nano Lett.* **2012**, 12, 5504.
- (25) Duan, H.; Fernández-Domínguez, A. I.; Bosman, M.; Maier, S. A.; and Yang, J. K. W. Nanoplasmonics: Classical down to the Nanometer Scale. *Nano Lett.* **2012**, 12, 1683.
- (26) Taylor, R. W.; Lee, T.-Ch.; Scherman, O. A.; Esteban, R.; Aizpurua, J.; Huang, F. M.; Baumberg, J. J.; and Mahajan, S. Precise Subnanometer Plasmonic Junctions for SERS within Gold Nanoparticle Assemblies Using Cucurbit[n]uril "Glue". *ACS Nano*, **2011**,5, 3878.
- (27) Danckwerts, M.; and Novotny, L. Optical Frequency Mixing at Coupled Gold Nanoparticles. *Phys. Rev. Lett.* **2007**, 98, 026104.
- (28) Savage, K. J.; Hawkeye, M. M.; Esteban, R.; Borisov, A. G.; Aizpurua, J.; Baumberg, J. J. Revealing the quantum regime in tunnelling plasmonics. *Nature* **2012**, 491, 574.
- (29) Scholl, J. A.; García-Etxarri, A.; Koh, A. L.; and Dionne, J. A. Observation of Quantum Tunneling between Two Plasmonic Nanoparticles. *Nano Lett.*, Articles ASAP, DOI: 10.1021/nl304078v.
- (30) Ward, D. R.; Hueser, F.; Pauly, F.; Cuevas, J. C.; Natelson, D. Optical rectification and field enhancement in a plasmonic nanogap. *Nature Nanotechnology* **2010**, 5, 732.
- (31) Zuolaga, J.; Prodan, E.; Nordlander, P. Quantum description of the plasmon resonances of a nanoparticle dimer. *Nano Lett.* **2009**, 9, 887.
- (32) Marinica, D. C.; Kazansky, A. K.; Nordlander, P.; Aizpurua, J.; and Borisov, A. G. Quantum

Plasmonics: Nonlinear Effects in the Field Enhancement of a Plasmonic Nanoparticle Dimer. *Nano Lett.* **2012**, 12, 1333.

- (33) Esteban, R.; Borisov, A. G.; Nordlander, P.; Aizpurua, J. Bridging quantum and classical plasmonics with a quantum-corrected model. *Nature Commun.* **2012**, 3, 825.
- (34) Quantum Plasmonics: Optical Properties and Tunability of Metallic Nanorods. Zuloaga, J.; Prodan, E.; and Nordlander, P. *ACS Nano* **2010**, 4, 5269.
- (35) García de Abajo, F. J. Nonlocal effects in the plasmons of strongly interacting nanoparticles, dimers, and waveguides. *Journal of Physical Chemistry C* **2008**, 112, 17983.
- (36) David, C.; and García de Abajo, F. J.; Spatial nonlocality in the optical response of metal nanoparticles. *Journal Phys. Chem. C* **2011**, 115, 19470.
- (37) McMahon, J. M.; Gray, S. K.; Schatz G. C. Nonlocal Optical Response of Metal Nanostructures with Arbitrary Shape. *Phys. Rev. Lett.* **2009**, 103, 097403.
- (38) McMahon, J. M.; Gray, S. K.; Schatz G. C. Optical Properties of Nanowire Dimers with a Spatially Nonlocal Dielectric Function. *Nano Lett.* **2010**, 10, 3473.
- (39) Ciraci, C.; Hill, R. T.; Mock, J. J.; Urzhumov, Y.; Fernández-Domínguez, A. I.; Maier, S. A.; Pendry, J. B.; Chilkoti, A.; Smith, D. R. Probing the Ultimate Limits of Plasmonic Enhancement. *Science* **2012**, 337, 1072.
- (40) Fernández-Domínguez, A. I.; Wiener, A.; García-Vidal, F. J.; Maier, S. A.; and Pendry, J. B. Transformation-Optics Description of Nonlocal Effects in Plasmonic Nanostructures. *Phys. Rev. Lett.* **2012**, 108, 106802.
- (41) Fernández-Domínguez, A. I.; Zhang, P.; Luo, Y.; Maier, S. A.; García-Vidal, F. J.; Pendry, J. B. Transformation-optics insight into nonlocal effects in separated nanowires. *Phys. Rev. B* **2012**, 86, 241110(R).

- (42) Toscano, G.; Raza, S.; Jauho, A.-P.; Mortensen, N. A.; Wubs, M. Modified field enhancement and extinction by plasmonic nanowire dimers due to nonlocal response. *Optics Express* **2012**, *20*, 4176.
- (43) Toscano, G.; Raza, S.; Xiao, S.; Wubs, M.; Jauho, A.-P.; Bozhevolnyi, S. I.; Mortensen, N. A. Surface-enhanced Raman spectroscopy (SERS): nonlocal limitations. *Opt. Lett.* **2012**, *37*, 2538.
- (44) Hao, E.; Schatz, G. C.; Electromagnetic fields around silver nanoparticles and dimers. *J. Chem. Phys.* **2004**, *120*, 357.
- (45) Romero, I.; Aizpurua, J.; Bryant, G. W.; García de Abajo, F. J. Plasmons in nearly touching metallic nanoparticles: singular response in the limit of touching dimers. *Optics Express* **2006**, *14*, 9988.
- (46) Jain, P. K.; El-Sayed, M. A. Plasmonic coupling in noble metal nanostructures. *Chem. Phys. Lett.* **2010**, *487*, 153.
- (47) Kottmann, J.; Martin, O. J. F. Plasmon resonant coupling in metallic nanowires. *Optics Express* **2001**, *8*, 655.
- (48) Atay, T.; Song, J.-H.; and Nurmikko, A. V. Strongly Interacting Plasmon Nanoparticle Pairs: From Dipole-Dipole Interaction to Conductively Coupled Regime. *Nano Lett.* **2004**, *4*, 1627.
- (49) Marhaba, S.; Bachelier, G.; Bonnet, Ch.; Broyer, M.; Cottancin, E.; Grillet, N.; Lerme, J.; Vialle, J.-L.; Pellarin, M. Surface plasmon resonance of single gold nanodimers near the conductive contact limit. *J. Phys. Chem. C* **2009**, *113*, 4349.
- (50) Schnell, M.; Garcia-Etxarri, A.; Huber, A. J.; Crozier, K.; Aizpurua, J.; Hillenbrand, R. Controlling the near-field oscillations of loaded plasmonic nanoantennas. *Nature Photonics* **2009**, *3*, 287.

- (51) Hentschel, M.; Dregely, D.; Vogelgesang, R.; Giessen, H.; Liu, N. Plasmonic Oligomers: The Role of Individual Particles in Collective Behavior. *ACS Nano* **2011**, *5*, 2042 (2011).
- (52) Banik, M.; El-Khoury, P. Z.; Nag, A.; Rodriguez-Perez, A.; Guarrotxena, N.; Bazan, G. C.; and Apkarian, V. A. Surface-Enhanced Raman Trajectories on a Nano-Dumbbell: Transition from Field to Charge Transfer Plasmons as the Spheres Fuse. *ACS Nano* **2012**, *6*, 10343.
- (53) Berthelot, J.; Bachelier, G.; Song, M.; Rai, P.; Colas des Francs, G.; Dereux, A.; and Bouchelier A. Silencing and enhancement of second-harmonic generation in optical gap antennas. *Optics Express* **2012**, *20*, 10498.
- (54) Manjavacas, A; García de Abajo, F. J. Robust plasmon waveguides in strongly interacting nanowire arrays. *Nano Lett.* **2009**, *9*, 1285.
- (55) Banholzer, M. J.; Li, S.; Ketter, J. B.; Rozkiewicz, D. I.; Schatz, G. C.; and Mirkin C. A. Electrochemical Approach to and the Physical Consequences of Preparing Nanostructures from Gold Nanorods with Smooth Ends. *J. Phys. Chem. C* **2008**, *112*, 15729.
- (56) Alexander, K. D.; Skinner, K.; Zhang, S.; Wei, H.; and Lopez, R. Tunable SERS in Gold Nanorod Dimers through Strain Control on an Elastomeric Substrate. *Nano Lett.* **2010**, *10*, 4488.
- (57) Osberg, K. D.; Rycenga, M.; Harris, N.; Schmucker, A. L.; Langille, M. R.; Schatz, G. C.; and Mirkin, C. A. Dispersible Gold Nanorod Dimers with Sub-5 nm Gaps as Local Amplifiers for Surface-Enhanced Raman Scattering. *Nano Lett.* **2012**, *12*, 3828.
- (58) Kottmann, J. P.; Martin, O. J. F. Retardation-induced plasmon resonances in coupled nanoparticles. *Optics Lett.* **2001**, *26*, 1096.
- (59) Halterman, K.; Elson, J. M.; and Singh, S. Plasmonic resonances and electromagnetic forces between coupled silver nanowires, *Phys. Rev. B* **2005**, *72*, 075429.

- (60) Jain, P. K.; El-Sayed, M. A. Plasmon Coupling in Nanorod Assemblies: Optical Absorption, Discrete Dipole Approximation Simulation, and Exciton-Coupling Model. *J. Phys. Chem. B* **2006**, 110, 18243.
- (61) Funston, A. M.; Novo, C.; Davis, T. J.; Mulvaney, P. Plasmon coupling of gold nanorods at short distances and in different geometries. *Nano Lett.* **2009**, 9, 1651.
- (62) Tabor, C.; Van Haute, D.; and El-Sayed, M. A. Effect of Orientation on Plasmonic Coupling between Gold Nanorods. *ACS Nano* **2009**, 3, 3670.
- (63) Lei, D. Y.; Aubry, A.; Luo, Y.; Maier, S. A.; Pendry J. B. Plasmon interaction between overlapping nanowires. *ACS Nano* **2011**, 5, 597.
- (64) Yannouleas, C.; Vigezzi, E.; Broglia, R.A. Evolution of the optical properties of alkali-metal microclusters towards the bulk: The matrix random-phase-approximation description. *Phys. Rev. B* **1993**, 47, 9849.
- (65) Marques, M. A. L.; and Gross, E. K. U. Time-Dependent Density Functional Theory. *Ann. Rev. of Phys. Chem.* **2004**, 55, 427.
- (66) Gunnarson, O.; and Lundqvist, B. I. Exchange and correlation in atoms, molecules, and solids by the spin-density-functional formalism. *Phys. Rev. B* **1976**, 13, 4274.
- (67) Hövel, H.; Fritz, S.; Hilger, A.; Kreibig, U.; Vollmer, M. Width of cluster plasmon resonances: Bulk dielectric functions and chemical interface damping. *Phys. Rev. B* **1993**, 48, 18178.
- (68) Appel, P.; Penn, D.R. Optical Properties of Small Metal Spheres: Surface Effects. *Phys. Rev. Lett.* **1983**, 50, 1316.
- (69) Klein-Wiele, J.-H.; Simon, P.; Rubahn, H.-G. Size-Dependent Plasmon Lifetimes and Electron-Phonon Coupling Time Constants for Surface Bound Na Clusters. *Phys. Rev. Lett.* **1998**, 80, 45.

- (70) Alcaraz de la Osa, R.; Sanz, J. M.; Saiz, J. M.; González, F.; and Moreno, F. Quantum optical response of metallic nanoparticles and dimers, *Optics Letters* **2012**, 37, 5015.
- (71) Parks, J.H.; McDonald, S.A. Evolution of the Collective-Mode Resonance in Small Adsorbed Sodium Clusters. *Phys. Rev. Lett.* **1989**, 62, 2301.
- (72) Borggreen, J.; Chowdhury, P.; Kebaïli, N.; Lundsberg-Nielsen, L.; Lützenkirchen, K.; Nielsen, M. B.; Pedersen, J.; Rasmussen, H. D.; Plasma excitations in charged sodium clusters. *Phys. Rev. B* **1993**, 48, 17507.
- (73) Reiners, T.; Ellert, C.; Schmidt, M.; and Haberland, H. Size Dependence of the Optical Response of Spherical Sodium Clusters. *Phys. Rev. Lett.* **1995**, 74, 1558.
- (74) Apell, P.; Ljungbert, Å. Red shift of surface plasmons in small metal particles. *Solid State Commun*, **1982**, 44, 1367.
- (75) Liebsch, A. Surface-plasmon dispersion and size dependence of Mie resonance: Silver versus simple metals. *Phys. Rev. B* **1993**, 48, 11317.
- (76) Feibelman, P.J. Surface electromagnetic fields. *Progress in Surface Science* **1982**, 12, 287.
- (77) Liebsch, A. Dynamical screening at simple-metal surfaces. *Phys. Rev. B* **1987**, 36, 7378.
- (78) Appel, P.; Ljungbert, Å.; Lundqvist, S. Non-Local Effects at Metal Surfaces. *Physica Scripta* **1984**, 30, 367.
- (79) Tiggesbäumker, J.; Köller, L.; Meiwes-Broer, K.-H.; and Liebsch, A. Blue shift of the Mie plasma frequency in Ag clusters and particles. *Phys. Rev. A* **1993**, 48, R1749.
- (80) Liebsch, A.; Schaich, W. L. Influence of a polarizable medium on the nonlocal optical response of a metal surface. *Phys. Rev. B* **1995**, 52, 14219.
- (81) Serra, L.; Rubio, A. Core Polarization in the Optical Response of Metal Clusters: Generalized Time-Dependent Density-Functional Theory. *Phys. Rev. Lett.* **1997**, 78, 1428.

- (82) Tsuei, K.-D.; Plummer, E. W.; Liebsch, A.; Kempa, K.; Bakshi, P. Multipole Plasmon Modes at a Metal Surface. *Phys. Rev. Lett.* **1990**, 64, 44.
- (83) Bennett, A. J. Influence of the Electron Charge Distribution on Surface-Plasmon Dispersion, *Phys. Rev. B* **1970**, 1, 203.
- (84) Pitarke, J. M.; Silkin, V. M.; Chulkov, E. V.; and Echenique, P. M. Theory of surface plasmons and surface-plasmon polaritons. *Rep. Prog. Phys.* **2007**, 70, 1.
- (85) Lermé, J.; Palpant, B.; Prével, B.; Pellarin, M.; Treilleux, M.; Vialle, J. L.; Perez A.; and Broyer, M. Quenching of the Size Effects in Free and Matrix-Embedded Silver Clusters. *Phys. Rev. Lett.* **1998**, 80, 5105.
- (86) Berciaud, S.; Cognet, L.; Tamarat, P; Lounis, B. Observation of Intrinsic Size Effects in the Optical Response of Individual Gold Nanoparticles. *Nano Lett.* **2005**, 5, 515.